However, we caution against interpreting the decadal variability as evidence of greenhouse gas warming. Whether the changes seen in the radiative balance in the last two decades are the result of natural variability or are a response to global change remains to be determined. A major step in understanding these changes is given in a companion paper in this issue (*21*), which offers a hypothesis for the link between these radiative balance changes and corresponding changes in the dynamical climate system, a system that appears to be much more variable than previously thought.

References and Notes

1. IPCC, *Climate 2001, The Scientific Basis*, J. T. Houghton *et al.* Eds. (Cambridge Univ. Press, Cambridge, 2001), pp. 87–91.
2. B. A. Wielicki *et al.*, *Bull. Am. Meteorol. Soc.* **76**, 2125 (1995).
3. B. A. Wielicki *et al.*, *Bull. Am. Meteorol. Soc.* **77**, 853 (1996).
4. The record of overlapping climate-quality satellite radiation data now extends from the Nimbus-7 mission, launched in 1978, through the current Earth Observing System Terra mission, launched in late 1999. Measurement of these fluxes in sufficient accuracy for climate research, however, is a serious challenge. Radiation fields vary greatly with spectral wavelength, time, latitude, longitude, and height from the surface of Earth; solar elevation angle; satellite viewing elevation angle; and satellite viewing azimuth angle relative to the solar plane (*2*). Achieving calibration accuracy of 1% or better as well as sufficient sampling of this eight-dimensional space is a major challenge to achieving data of climate accuracy of order 1 Wm^{-2}.
5. B. R. Barkstrom *et al.*, *Bull. Am. Meteorol. Soc.* **70**, 1254 (1989).
6. Nonscanning radiometers view the entire hemisphere of radiation but with a roughly 1000-km field of view. Scanning radiometers view radiance from a single direction and must estimate the hemispheric emission or reflection. Because of this fundamental difference, scanner and NS radiometers are each treated as a single group for the anomalies. For details on the radiometers and data sources used in this study, see (*19*).
7. P. Minnis *et al.*, *Science* **259**, 1411 (1993).
8. Narrowband atmospheric window and sounding instruments attempt to estimate the full broadband LW fluxes with the use of regressions and radiative modeling approaches. For results using the latest versions of these data sets, see (*19*).
9. The ERBS active cavity NS calibration record was examined for changes in instrument channel gains and offsets, for SW filter dome transmission loss over time, and for nonuniformity of dome transmission. The calibration uncertainties found were less than 0.5 Wm^{-2}, and the time variations in ERBS calibration were inconsistent with the tropical mean SW and LW flux anomalies in Figs. 1 through 4. For details, see (*19*).
10. T. Wong *et al.*, *J. Clim.* **13**, 4256 (2000).
11. There is no significant change in the ERBS spacecraft orbit during the record, so the sudden appearance of the semi-annual cycle after 1993 cannot be explained by diurnal cycle sampling errors causing seasonal cycle errors. The ERBS spacecraft orbit precesses through 12 hours of local time in approximately 36 days. Because Earth is viewed on both sides of the orbit 12 hours apart in the tropics, the full diurnal cycle is covered every 36 days or about 10 times per year. Diurnal cycle sampling errors across the tropics estimated by sub-sampling hourly geostationary data gave values of 0.14, 0.24, and 0.37 Wm^{-2} for LW fluxes from the TRMM, ERBS scanner, and ERBS NS data, respectively. The corresponding errors for SW fluxes are larger at 0.9, 1.6, and 1.7 Wm^{-2} (*22*, *23*). We conclude that large (5 Wm^{-2}) changes in seasonal cycle of tropical radiation have occurred in the decade of the 1990s.
12. SSTs were the NCEP/Reynolds reconstructed SSTs (*24*), except for the HadAM3 model, which used version 3.1 of the UK Met Office Global Sea Ice Coverage and Sea Surface Temperature (GISST). [experiments provided by and described in (*14*)].
13. V. D. Pope *et al.*, *Clim. Dyn.* **16**, 123 (2000).
14. D. M. H. Sexton *et al.*, *Clim. Dyn.* **17**, 669 (2001).
15. J. T. Kiehl *et al.*, *J. Clim.* **11**, 1131 (1998).
16. N. C. Lau, *J. Clim.*, **14** 2846 (2001).
17. C. T. Gordon *et al.*, *J. Clim.* **13**, 2239 (2000).
18. R. E. Kistler *et al.*, *Bull. Am. Meteorol. Soc.* **82**, 247 (2001).
19. Supplemental material is available on *Science* Online at www.sciencemag.org/cgi/content/full/295/5556/841/DC1.
20. D. J. Gaffen *et al.*, *Science* **287**, 1242 (2000).
21. J. Chen, B. W. Carlson, A. D. Del Genio, *Science* **295**, 838 (2002).
22. D. F. Young *et al.*, *J. Appl. Met.* **37**, 572 (1998).
23. T. Wong *et al.*, *AMS 12th Symposium on Global Change*, 14 to 18 January 2001, Albuquerque, NM (American Meteorological Society, Boston, 2001).
24. T. M. Smith *et al.*, *J. Clim.* **9**, 1403, (1996).
25. The Nimbus 7 satellite is in local noon orbit, which is highly biased for solar fluxes. The Scanner for Radiation Budget (ScaRaB)/Meteor satellite requires about 7 months to precess through the diurnal cycle, causing diurnal cycle sampling errors to occur in seasonal cycles. The ScaRaB/Resurs and CERES/Terra data are sun-synchronous satellites fixed at local sampling times near 10 to 11 a.m. Further research is required to achieve accurate diurnal cycle corrections for SW fluxes using these satellites.

26. We would like to thank the CERES science, algorithm, and data management teams, whose contributions were essential to continuing and improving this key climate radiation data set. The surprising initial TRMM CERES data was the motivation for this analysis. We would like to thank the NASA Langley Atmospheric Sciences Data Center for providing the ERBE S-4 and CERES ES-4 data sets. The NCEP–NCAR 50-Year Reanalysis data were obtained at http://wesley.wwb.noaa.gov/reanalysis.html. G. Gibson and D. Young provided reviews that greatly helped the clarity of the paper. R. B. Lee III, G. L. Smith, J. Paden, and K. Bush provided a careful review of the ERBS NS calibration record. Funding for this research was provided by the NASA Earth Sciences Enterprise. The work at the Hadley Centre was supported by the UK Department for Environment, Food and Rural Affairs under contract PECD/7/12/37.

29 August 2001; accepted 3 January 2002

Distinguishing Inchworm and Hand-Over-Hand Processive Kinesin Movement by Neck Rotation Measurements

Wei Hua,[1] Johnson Chung,[2] Jeff Gelles[1,2]*

The motor enzyme kinesin makes hundreds of unidirectional 8-nanometer steps without detaching from or freely sliding along the microtubule on which it moves. We investigated the kinesin stepping mechanism by immobilizing a *Drosophila* kinesin derivative through the carboxyl-terminal end of the neck coiled-coil domain and measuring orientations of microtubules moved by single enzyme molecules at submicromolar adenosine triphosphate concentrations. The kinesin-mediated microtubule-surface linkage was sufficiently torsionally stiff ($\geq 2.0 \pm 0.9 \times 10^{-20}$ Newton meters per radian^2) that stepping by the hypothesized symmetric hand-over-hand mechanism would produce 180° rotations of the microtubule relative to the immobilized kinesin neck. In fact, there were no rotations, a finding that is inconsistent with symmetric hand-over-hand movement. An alternative "inchworm" mechanism is consistent with our experimental results.

The motor enzyme kinesin moves membrane-bound organelles along microtubules in eukaryotic cells (*1*). Microtubule-based movements of organelles in vivo may be driven by as few as one motor enzyme molecule (*2*). Observations of the movement of single kinesin molecules in vitro demonstrate that the enzyme is well adapted to functioning as an isolated single molecule in living cells. First, the enzyme is processive: The kinesin undergoes multiple catalytic turnovers without detaching from the microtubule (*3*, *4*), facilitating efficient organelle transport over long distances (*5*). Second, the duty ratio of kinesin is high: The enzyme cannot freely slide in the direction of the microtubule axis during most or all of its enzymatic cycle (*6*, *7*) and thus is able to move forward even when opposed by the substantial elastic forces imposed by mechanical obstructions to organelle movements inside cells.

The mechanism by which single kinesin molecules achieve processive, high–duty-ratio movement is not well understood. Both of the enzyme's two identical head domains are required for such movement: the kinesin one-headed homolog KIF1A is processive but has low duty ratio (*8*–*10*), and truncated kinesin constructs with only one head have low duty

[1]Biophysics and Structural Biology Program, [2]Biochemistry Department, Brandeis University, Waltham, MA 02454–9110, USA.

*To whom correspondence should be addressed. E-mail: gelles@brandeis.edu

ratios and little or no processivity [(*7*, *11*, *12*) but see also (*13*)]. These observations suggest that kinesin retains its grip on the microtubule through a mechanism in which head movement is coordinated so that at least one of the two heads is tightly bound to the microtubule at every stage of the catalytic cycle. It has been hypothesized that the two heads alternately move past each other (Fig. 1A). In such a symmetric hand-over-hand mechanism, the three-dimensional structure of the kinesin-microtubule complex is identical at the beginning of each adenosine triphosphate (ATP) hydrolytic cycle, except that in each cycle the two subunits (and therefore the two heads) swap places (*14*–*18*). Consequently, the neck coiled-coil domain, which links the heads together, rotates 180° around its axis for every 8-nm step (Fig. 1A, magenta arrows) (*18*). Analogous alternating-sites mechanisms have been hypothesized to explain the behavior of other dimeric processive motor enzymes such as myosin V (*19*) and Rep helicase (*20*). An alternative hypothesis is that kinesin head movement is coordinated through an "inchworm" mechanism (Fig. 1B) (*21*–*23*) in which the structure of the kinesin-microtubule complex is again identical at the beginning of each cycle but the two heads do not swap places. Thus, there is no net neck rotation in each cycle (Fig. 1B, magenta arrows). Such a mechanism differs fundamentally from the symmetric hand-over-hand type in that the two identical subunits of the kinesin homodimer are maintained in different environments and therefore have nonequivalent enzymatic cycles.

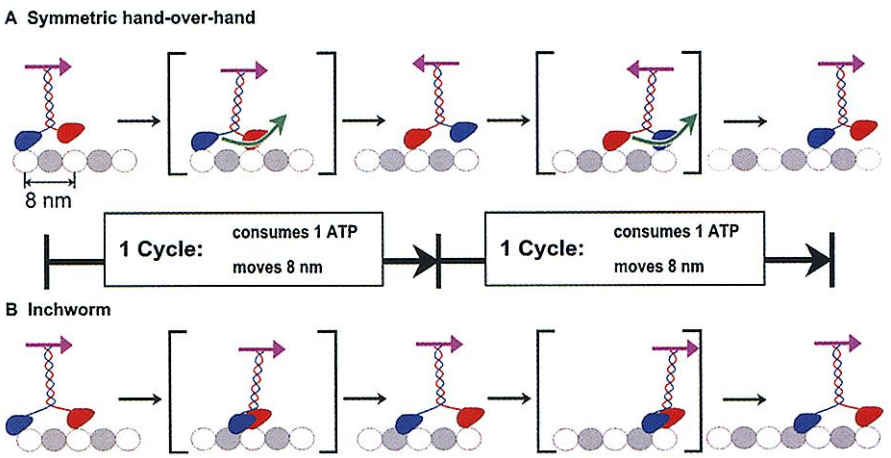

Fig. 1. Examples of two alternative classes of mechanisms for processive, high–duty ratio movement by kinesin. Kinesin hydrolyzes one molecule of ATP and moves 8 nm in a single catalytic cycle. In both examples, the enzyme moves along a microtubule protofilament consisting of alternating α (gray) and β (white) tubulin subunits in such a way that at least one of the two identical head domains (colored red and blue for identification) is bound to the microtubule at all times. In a symmetric hand-over-hand mechanism (**A**), the two heads undergo identical chemomechanical reaction sequences out of phase with each other so that the heads alternate in the leading and trailing positions at the beginnings of consecutive cycles. Consequently, each cycle changes the orientation (magenta arrow) of the neck coiled-coil domain by 180°. By contrast, in an inchworm mechanism (**B**), the two heads retain their nonequivalent positions at the beginnings of each successive cycle (in the example shown here, the red head is always in front of the blue). The cycle of chemomechanical reactions is thus different in the two heads, and the neck orientation does not change from the beginning of one cycle to the next. Postulation of particular structures or mechanical properties for the intermediates formed during the cycles (for example, those shown in brackets) is not necessary to differentiate between the two types of mechanisms because the types are defined only by the structures of the kinesin-microtubule complex at the beginning of successive cycles.

To differentiate between these two types of mechanisms, we immobilized kinesin molecules by the distal end of the neck and examined the extent of microtubule rotation relative to the immobilized neck (Fig. 2A). The biotinated kinesin derivative K448-BIO (*7*, *11*, *15*, *24*) was attached to a streptavidin-coated glass cover slip (*25*) at low surface density, and the orientations of microtubules interacting with the surface-attached enzyme molecules were then observed by light microscopy, a modification of the method used by Hunt and Howard (*26*) to study kinesin torsional stiffness. In the presence of 1 to 4 mM concentrations of the kinesin inhibitor adenylyl imidodiphosphate (AMP-PNP), 100% of the microtubules that remained bound at the surface pivoted around a single point (Fig. 2B), demonstrating that they are attached to single molecules of kinesin (*3*, *27*).

All microtubules pivoted over a limited range of orientations (Fig. 2C); σ_0, the root-mean-square orientation angle, was 44° ± 18° (mean ± SD) (Table 1). Assuming that the linkage of the microtubule to the surface through kinesin and streptavidin behaves like a simple torsion spring, the linkage torsional stiffness (K) can be calculated from the equipartition theorem (*26*, *28*) as $\langle kT/\sigma_0^2 \rangle = 2.0 \pm 0.9 \times 10^{-20}$ N m rad^{-2}, where k is the Boltzmann constant, T is the absolute temperature, and the angle brackets indicate that the quantity is the average over the sample of microtubules analyzed (*29*). When the kinesin molecules were instead bound nonspecifi-

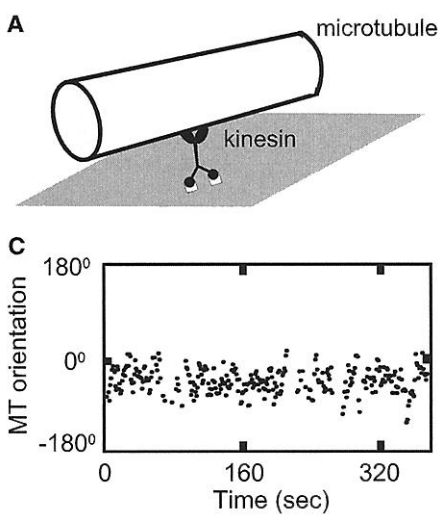

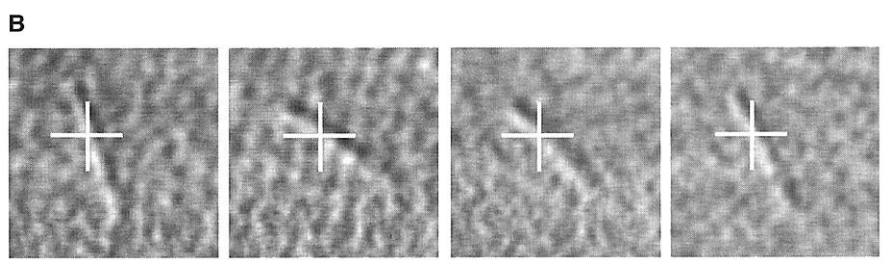

Fig. 2. Torsional Brownian motion of a microtubule bound to a single surface-attached kinesin molecule in the presence of 1 mM AMP-PNP. Schematic (**A**) illustrates the experimental sample in which a microtubule (cylinder) is bound to the head(s) of a kinesin molecule specifically attached to a streptavidin (white squares)–coated glass cover slip (gray) through one or both biotin (black circles) moieties incorporated at the distal end of the neck coiled coil (*27*). Light microscope images (33.3-ms acquisition time; 1-s interval between images shown) of a 1.8-μm-long microtubule (**B**) demonstrate that it pivots around a single point (cross) on the surface through a restricted range of angles (*36*) (**C**). MT, microtubule.

Table 1. Movement of microtubules interacting with single kinesin molecules.

Nucleotide	1 or 4 mM AMP-PNP	400 nM ATP	5 nM ATP
Number of microtubules analyzed	17	19	24
Total duration (s)	4,595	2,091	29,128
Width of orientation distribution			
RMS orientation, $\langle\sigma_\theta\rangle \pm$ SD*	44° ± 18° (N = 17)	24° ± 10° (N = 19)	31° ± 11° (N = 24)
Fraction of measurements with $\theta_0 - 90° < \theta < \theta_0 + 90°$†	99.3%	100%	99.9%
Translation velocity (nm s^{-1})			
Measured ± SE (*38*)*	0.05 ± 0.01 (N = 5)‡§	5.3 ± 0.9 (N = 19)	0.09 ± 0.01 (N = 8)‡§
Expected	0	7.1‖	0.09‖
Total 8-nm steps¶	Not applicable	1,385	328‡

*Average of values measured for N microtubules. †θ_0 is the microtubule orientation, θ, averaged over the whole data record. ‡All data records shorter than 350 s [the total duration of which was 2411 s (AMP-PNP) or 4246 s (5 nM ATP)] were excluded to increase precision. §Significantly different from each other ($P < 0.016$). ‖Calculated as $(V_{max}/K_m)A$, where A is the ATP concentration, K_m = 46 μM, and V_{max} = 819 nm s^{-1} (*15*). ¶Translation velocity multiplied by total duration divided by 8 nm.

cally to the surface, the microtubules exhibited Brownian rotation over >360° (Fig. 3), as observed previously with full-length kinesin (*26*), suggesting that the restricted torsional Brownian motion observed with specifically attached enzyme molecules is not due to obstruction of microtubule movement by surface irregularities. Taken together, the results illustrated in Figs. 2 and 3 suggest that the head-microtubule connection, the neck-streptavidin connection, and the enzyme molecule itself all are torsionally stiff.

To determine whether single catalytic cycles of kinesin entail net rotation of the neck coiled coil relative to the microtubule, we examined orientations of microtubules moved by single enzyme molecules at 400 nM ATP, a concentration 115-fold lower than the Michaelis constant (K_m) (*15*). Under these conditions, the kinesin spends >99% of its time poised at the beginning of its catalytic cycle, waiting for substrate to bind. Individual catalytic turnovers (which have a mean duration of ~10 ms) are well separated by long intervals (which have a mean duration of >1 s) in which the enzyme remains bound to a fixed position on the microtubule (*15*). In these experiments, microtubules glide past a single pivot point on the cover slip surface (Fig. 4A) and release from the surface when the microtubule end reaches this same single pivot point (*3*). The width of the distribution of microtubule orientations in 400 nM ATP was similar to that seen in AMP-PNP (Table 1). Thus, the cover slip–microtubule linkage has a well-defined equilibrium orientation and does not freely swivel when the kinesin molecule is poised at the beginning of the cycle. The calculated rigidity of the linkage is sufficiently high that the torsional relaxation time for a 2-μm-long microtubule pivoting around its center to reach its equilibrium position is <1 s (*30*). We collected movement records corresponding to >1000 8-nm steps (Table 1); if the catalytic cycle entails a 180° rotation of the neck relative to the microtubule, the short relaxation time dictates that these records would contain numerous observations of 180° microtubule rotations. Strikingly, no such rotations were observed; the microtubules were always oriented in approximately the same direction (Fig. 4B). This observation directly conflicts with the behavior predicted for a symmetric hand-over-hand mechanism.

To further improve our ability to detect even small (<<180°) neck rotations associated with kinesin steps, we repeated the experiments at 5 nM ATP, a condition in which kinesin steps are separated by an average interval of 89 s (Fig. 4C and Table 1). Again, no 180° rotations were observed, even though we examined microtubule movements corresponding to >300 8-nm steps. No experimentally significant discontinuities of any size were detected in most microtubule orientation records, indicating that step-associated rotations, if any, are considerably smaller than the $\langle\sigma_\theta\rangle$ of 31° (Table 1) for these records.

For data at both 5 and 400 nM ATP, the fraction of measured orientations falling within ± 90° from the mean is >99% (Table 1), as would be expected from a mechanism in which no rotation occurs, not ~50%, as predicted by the symmetric hand-over-hand mechanism.

No systematic changes in σ_θ with time were observed in individual microtubule movement records, even for those at 400 nM ATP in which the microtubule moved from pivoting near the microtubule center to pivoting at or near its end. These observations are consistent with our proposal that the extent of pivoting is limited by the surface linkage torsional stiffness; they are inconsistent with a possible alternative interpretation in which pivoting is restricted by collision of the microtubule ends with the surface. To confirm that the limited rotation we observed was not a consequence of some unknown geometrical constraint specific to the microtubule pivoting experiments used here, we independently measured the extent of kinesin neck rotation from one 8-nm step to the next at subsaturating ATP concentrations by observing the motion of asymmetric bead aggregates moved by kinesin along immobilized microtubules (*31*). Again, step-associated neck rotation was found to be small or zero. The same result was obtained in further experiments in which the rotation of spherical fluorescent beads coupled to single kinesin molecules moving on immobilized microtubules or demembranated axonemes was monitored by fluorescence polarization techniques (*32*).

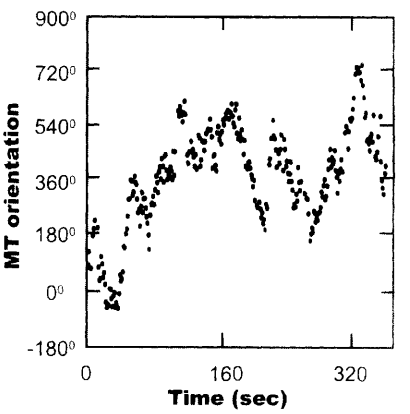

Fig. 3. Rotational Brownian motion in 1 mM AMP-PNP of a microtubule bound to a kinesin molecule nonspecifically adsorbed to the cover slip surface (*37*). Nonspecific attachment was achieved by saturating the streptavidin-coated surface with excess biotin (*27*) and then increasing the enzyme concentration 80-fold and the incubation time threefold over that used for specific attachment. A range of rotation larger than 360° was measured in 10 of 10 such microtubules studied. MT, microtubule.

The observation that the kinesin neck coiled coil does not rotate 180° from the beginning of one step to the beginning of the next is inconsistent with the symmetric hand-over-hand model (Fig. 1A), in which the two heads swap leading and trailing positions in consecutive cycles. This conclusion depends only on the essential feature of this model: that the three-dimensional structure of the kinesin-microtubule complex is identical (except for translation along the microtubule lattice and the interchange of the two heads in alternate steps) at the beginning of each cycle. Thus, the conclusion is independent of any assumptions about the details of the movements that occur transiently during the cycle. For example, it is immaterial whether one assumes that the trailing head always passes to the same side of the leading one (Fig. 1A, green arrows), alternates the sides on which it passes, or chooses sides randomly (*18*).

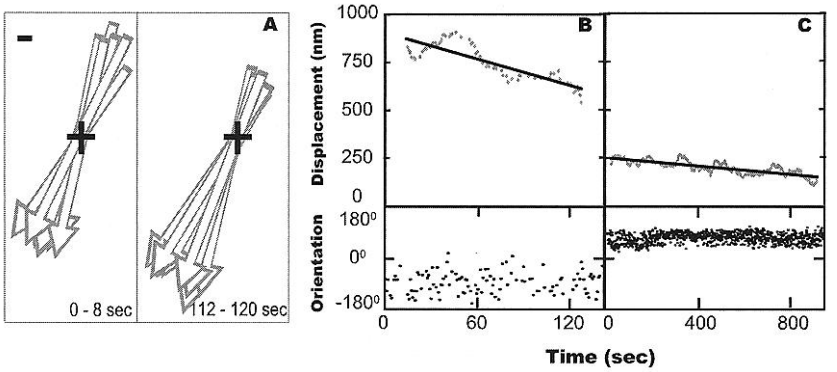

Fig. 4. Movement of microtubules by specifically surface-attached single kinesin molecules in the presence of ATP. (**A**) Overlaid traces at 1-s intervals of a microtubule (arrows) in 400 nM ATP pivoting around a single point (cross) on the cover slip surface. Panels show the same microtubule in two different time periods separated by 104 s (*37*). Scale bar, 100 nm. (**B** and **C**) Displacement and orientation records of two microtubules in 400 (B) and 5 (C) nM ATP. Displacement is measured as the length of the microtubule segment between the trailing end and the pivot point. Displacement records are filtered with 40-point (B) and 100-point (C) mean filters and give linear fits (lines) with slopes of 2.6 (A) and 0.1 (B) nm s^{-1}. Orientation records are not filtered. Note different time scales in (B) and (C).

Our observations instead are consistent with the inchworm type of mechanism (Fig. 1B), in which the structure of the kinesin-microtubule complex is identical at the beginning of every cycle and the heads do not swap places.

Both mechanisms shown in Fig. 1 adhere to the simplifying assumption that the three-dimensional geometry of the kinesin-microtubule complex is identical at the beginning of each 8-nm step. However, if we drop this assumption, we can consider yet a third type of mechanism (*21*), in which the neck-linker domain (or any other structure through which the heads are attached to the surface in our experiments) exists in two distinct, stable conformations that alternate in successive enzymatic cycles. In that case, hand-over-hand alternation of the head positions in successive cycles can produce the ~0° microtubule rotation with each step observed in our experiments, provided that the two conformations differ in precisely such a way as to cancel the 180° reorientation induced by head alternation. We call this type of mechanism *asymmetric* hand-over-hand to emphasize that the three-dimensional structures at the beginning of consecutive 8-nm steps are different (i.e., not symmetry related). A concrete example of such a mechanism is that proposed by Hoenger *et al.* (*33*). To be consistent with the known properties of kinesin movement, the two postulated linker conformations must satisfy stringent criteria in addition to nearly exact compensation for the rotation caused by head interchange: (i) The angle between the microtubule axis and the coiled coil must not differ in the two conformations; otherwise, consecutive steps observed in bead movement experiments would not be uniformly 8 nm as observed (*14*, *15*, *34*). (ii) The equatorial angle of the coiled coil around the microtubule circumference also must not change, because beads moved along immobilized microtubules by single kinesin molecules do not wobble from side to side in alternate steps (*11*, *31*). The radii of the beads used in the cited experiments are sufficiently large (>50 nm) that changes of even ~5° in either angle would likely be detected (*11*). (iii) A high-energy barrier must block any interconversion of the two conformations that is not accompanied by catalytic turnover. Even spontaneous interconversion rates of 10^{-3} s^{-1} would produce detectable 180° rotations of microtubules in both the AMP-PNP and the limiting ATP experiments summarized in Table 1. (iv) The two stable structures must unfailingly (>99% of the time) alternate with each adenosine triphosphatase (ATPase) turnover; otherwise, 180° rotations would be observed in the 400 nM ATP experiments (Table 1). Thus, although our experimental results do not rigorously exclude an asymmetric hand-over-hand mechanism, we regard as improbable the existence of two structures that simultaneously satisfy all of the requirements outlined above.

In an inchworm mechanism, the two heads of kinesin remain in different environments (one always leading, the other always trailing) during continuous processive movement. The difference in environment implies that the chemical reactions taking place in the ATPase active sites of the two heads need not be identical. Indeed, the reactions cannot be identical—in a single cycle of the inchworm mechanism, each of the two heads moves forward 8 nm, yet only a single molecule of ATP is consumed (Fig. 1B) (*14*, *15*). Thus, the inchworm mechanism makes the unorthodox prediction that only one of kinesin's two heads is an active ATPase during processive movement. Observations of ATP-stimulated adenosine diphosphate (ADP) release from kinesin-microtubule complexes [for example, in (*17*)] are sometimes taken as supporting hand-over-hand mechanisms, in which both heads hydrolyze ATP. However, such results are also consistent with processive movement driven by ATP hydrolysis in only one of the two heads, given that ATP-stimulated ADP release has been demonstrated only in the pre–steady-state reactions that occur immediately upon mixing of kinesin with ATP and/or microtubules. Such reaction steps are thus not proven to be part of the catalytic cycle for steady-state processive movement. The data presented here, taken together with that from previous studies of kinesin function, strongly support an inchworm mechanism for the processive, high–duty-ratio movement of kinesin dimers. Because hand-over-hand mechanisms proposed for other processive motor enzymes may be based in part on analogy to kinesin, the failure of kinesin to conform to predictions of the hand-over-hand hypothesis suggests that reevaluation of the evidence supporting hand-over-hand movement by other motor enzymes may be necessary.

References and Notes

1. L. S. Goldstein, A. V. Philp, *Annu. Rev. Cell Dev. Biol.* **15**, 141 (1999).
2. M. A. Welte, S. P. Gross, M. Postner, S. M. Block, E. F. Wieschaus, *Cell* **92**, 547 (1998).
3. J. Howard, A. J. Hudspeth, R. D. Vale, *Nature* **342**, 154 (1989).
4. D. D. Hackney, *Nature* **377**, 448 (1995).
5. J. Howard, *Nature* **389**, 561 (1997).
6. K. Svoboda, S. M. Block, *Cell* **77**, 773 (1994).
7. E. C. Young, H. K. Mahtani, J. Gelles, *Biochemistry* **37**, 3467 (1998).
8. M. Kikkawa, Y. Okada, N. Hirokawa, *Cell* **100**, 241 (2000).
9. Y. Okada, N. Hirokawa, *Science* **283**, 1152 (1999).
10. Y. Okada, N. Hirokawa, *Proc. Natl. Acad. Sci. U.S.A.* **97**, 640 (2000).
11. E. Berliner, E. C. Young, K. Anderson, H. K. Mahtani, J. Gelles, *Nature* **373**, 718 (1995).
12. W. O. Hancock, J. Howard, *J. Cell Biol.* **140**, 1395 (1998).
13. Y. Inoue, A. H. Iwane, T. Miyai, E. Muto, T. Yanagida, *Biophys. J.* **81**, 2838 (2001).
14. M. J. Schnitzer, S. M. Block, *Nature* **388**, 386 (1997).
15. W. Hua, E. C. Young, M. L. Fleming, J. Gelles, *Nature* **388**, 390 (1997).
16. B. J. Schnapp, B. Crise, M. P. Sheetz, T. S. Reese, S. Khan, *Proc. Natl. Acad. Sci. U.S.A.* **87**, 10053 (1990).
17. D. D. Hackney, *Proc. Natl. Acad. Sci. U.S.A.* **91**, 6865 (1994).
18. J. Howard, *Annu. Rev. Physiol.* **58**, 703 (1996).
19. A. D. Mehta *et al.*, *Nature* **400**, 590 (1999).
20. I. Wong, T. M. Lohman, *Science* **256**, 350 (1992).
21. S. M. Block, K. Svoboda, *Biophys. J.* **68**, 230S (1995).
22. R. A. Cross, *J. Muscle Res. Cell Motil.* **16**, 91 (1995).
23. F. Kozielski *et al.*, *Cell* **91**, 985 (1997).
24. E. C. Young, E. Berliner, H. K. Mahtani, B. Perez-Ramirez, J. Gelles, *J. Biol. Chem.* **270**, 3926 (1995).
25. E. Berliner *et al.*, *J. Biol. Chem.* **269**, 8610 (1994).
26. A. J. Hunt, J. Howard, *Proc. Natl. Acad. Sci. U.S.A.* **90**, 11653 (1993).
27. The enzyme preparation used in these studies is monodisperse and uniformly dimeric (*24*). Cover slip flow cells with bound K448-BIO and microtubules were prepared as described (*7*), with the following modifications: Methylcellulose was omitted, and tubulin was polymerized for only 5 min in the absence of taxol and then for 20 min in its presence to produce short microtubules (the median microtubule length used in these experiments was 2.7 μm). 0.4 fmol of enzyme was added to each flow cell, resulting in at most approximately one active enzyme molecule per μm^2, assuming complete attachment. Because a single kinesin molecule is sufficient to retain a microtubule at the surface in the presence of AMP-PNP, the result that all observed surface-retained microtubules pivoted at a single point on the surface demonstrated that essentially all microtubules were bound to single enzyme molecules (*3*). Incubation of the streptavidin-coated cover slip surface with excess biotin before enzyme addition reduced the surface density of pivoting microtubules to <2.4% of that observed without excess biotin, demonstrating that most or all of the kinesin molecules were surface attached through specific

Partitioning of the Matrix Fraction of the Golgi Apparatus During Mitosis in Animal Cells

Joachim Seemann, Marc Pypaert, Tomohiko Taguchi, Jörg Malsam, Graham Warren*

The Golgi apparatus is partitioned during mitosis in animal cells by a process of fragmentation, dispersal, and reassembly in each daughter cell. We fractionated the Golgi apparatus in vivo using the drug brefeldin A or a dominant-negative mutant of the Sar1p protein. After these treatments, Golgi enzymes moved back to the endoplasmic reticulum, leaving behind a matrix of Golgi structural proteins. Under these conditions, cells still entered and exited mitosis normally, and their Golgi matrix partitioned in a manner very similar to that of the complete organelle. Thus, the matrix may be the partitioning unit of the Golgi apparatus and may carry the Golgi enzyme–containing membranes into the daughter cells.

There are two popular models of the partitioning of the Golgi apparatus during mitosis in animal cells, which differ as to the nature of the partitioning units. The first model argues that the units are the Golgi membranes themselves, which break down at the onset of mitosis, yielding vesicle clusters and shed vesicles, either or both of which have been suggested as the means of inheriting the Golgi (*1–4*). The second model argues that the partitioning units are endoplasmic reticulum (ER) membranes, with the Golgi merging with the ER during prometaphase and emerging from it during telophase (*5*).

Attempts to distinguish between these two models have yielded contradictory results, particularly when Golgi enzymes have been used to trace the partitioning process (*1–3*, *5–7*). We therefore decided to focus on another class of markers, the Golgi matrix proteins, which include the golgin and GRASP families of vesicle tethering and cisternal stacking proteins (*8*). In the presence of brefeldin A (BFA), these matrix proteins can be separated from Golgi enzymes (*9*). The enzymes move to the ER, whereas matrix proteins appear in dispersed punctate structures that may become associated with ER export sites (*10*). Separation also occurs in the presence of a dominant-negative Sar1p protein, which traps the Golgi enzymes as they cycle through the ER (*1*, *5*, *11*, *12*). The matrix proteins slowly disperse throughout the cytoplasm, although there is evidence that some become associated with the ER (*13*), especially when a guanosine diphosphate–restricted form of a dominant-negative Sar1p is used (*10*).

When BFA-treated cells are injected with Sar1dn (a guanosine triphosphate–restricted form) and the BFA is washed out, the matrix proteins re-form a ribbon-like structure near the nucleus that resembles the Golgi apparatus even though Golgi enzymes are trapped in the ER (*9*). This suggests that the matrix may provide a scaffold for the Golgi enzyme–containing membranes (*9*). The matrix might also provide the means of partitioning the Golgi during mitosis, so we asked whether it would partition between daughter cells in the absence of the enzyme-containing membranes that normally populate it. We first tested the effect of BFA on progression through mitosis, using time-lapse microscopy of synchronized normal rat kidney (NRK) cells. BFA had no effect on the time elapsed from prometaphase to telophase/G_1 [control cells, 32 ± 2 (SD) min; BFA-treated cells, 33 ± 2 (SD) min] when added about 90 min before the mitotic peak, which is sufficient time to separate enzyme and matrix proteins before entry into mitosis (*14*).

Unsynchronized cells were then treated with BFA for 90 min, fixed, and labeled for the Golgi matrix marker GM130, microtubules, and DNA, to determine the mitotic phase (*15*). After treatment with BFA, the matrix fraction of the interphase Golgi was a little more fragmented, but

Table 1. Distribution of GM130 in mitotic NRK cells. BFA was added, 90 min before fixation, to exponentially growing NRK cells, which were then labeled with polyclonal antibodies to GM130 and secondary antibodies coupled to Alexa Fluor 488. Total fluorescence on each side of the equatorial plate in metaphase cells and in each daughter cell pair in telophase was quantified, and background fluorescence was subtracted. For each pair of values, the percentage deviation from 50% was calculated, and the median deviation was determined from the number (n) of pairs evaluated.

	Median deviation from equality	
	+BFA	Control
Metaphase	2.8% (n = 87)	3.2% (n = 79)
Telophase/G_1	3.8% (n = 56)	3.7% (n = 57)

Department of Cell Biology, Ludwig Institute for Cancer Research, Yale University School of Medicine, 333 Cedar Street, Post Office Box 208002, New Haven, CT 06520–8002, USA.

*To whom correspondence should be addressed. E-mail: graham.warren@yale.edu

biotin-streptavidin linkages. Because the linkage length is <1% that of the microtubule, the observed pivoting must occur around an axis inclined no more than ~2° from the surface normal. Because individual linkages presumably project from the surface over a broader range of inclination angles, the observation that all microtubules pivot around the surface normal through similar angular ranges suggests that the linkage has a significant bending compliance.

28. Measurement of K from thermal fluctuations requires that the orientational correlation time be much longer than the single-frame acquisition time. We verified that this requirement was fulfilled by confirming that the variance of randomly selected data records was reduced by <10% when angle records sampled at 30 Hz were filtered with a four-point mean filter. For some microtubules, small (~11° to 22°) stochastic shifts in the equilibrium position occurred at ~50-s intervals, increasing the measured variance. Thus, the calculated value of K somewhat underestimates the true stiffness of the microtubule-kinesin–cover slip linkage.
29. Torsional stiffness of similar magnitude was previously observed in single-molecule measurements of the orientation of F-actin attached to the F_1-ATPase (*35*). As in our experiments, the filament-surface linkage in that study includes a coiled coil (the γ subunit) and a biotin-streptavidin linkage.
30. The relaxation time is calculated as $\tau = (1/3)c_\perp(L_1^3 + L_2^3)/K$, where $c_\perp = 9.4 \times 10^{-3}$ N s m^{-2} is the drag coefficient per unit length for translation perpendicular to the microtubule axis and L_1 and L_2 are the lengths of the two ends of the microtubule (*26*). The median τ values for microtubules in the 1 mM AMP-PNP, 400 nM ATP, and 5 nM ATP experiments reported here are 1.0 ± 1.4, 0.8 ± 1.3, and 0.2 ± 0.6 (± SD) s. These values are consistent with independent estimates of the relaxation times derived from autocorrelation analysis of the microtubule orientation records.
31. W. Hua, J. Chung, J. Gelles, manuscript in preparation.
32. J. Chung, W. Hua, J. Gelles, manuscript in preparation.
33. A. Hoenger *et al.*, *J. Mol. Biol.* **297**, 1087 (2000).
34. K. Svoboda, C. F. Schmidt, B. J. Schnapp, S. M. Block, *Nature* **365**, 721 (1993).
35. H. Noji, R. Yasuda, M. Yoshida, K. Kinosita Jr., *Nature* **386**, 299 (1997).
36. Unlabeled microtubules were visualized by differential interference contrast microscopy, movements were recorded on videotape (30 frames s^{-1}), and the positions of both microtubule ends were measured in single frames, as described (*7*). The measured end positions were then used to compute the orientation of the microtubule relative to an arbitrary reference orientation. Microtubules were chosen for analysis only if the pivot point remained sufficiently far from the center or the torsional relaxation time was sufficiently long that the two ends could be unambiguously distinguished. Orientations were typically measured at ~1-s intervals, but the sampling interval was occasionally reduced to 33.3 ms to verify reliable end tracking.
37. A movie showing microtubule movement under this condition is available as supplementary material on *Science* Online at www.sciencemag.org/cgi/content/full/295/5556/844/DC1.
38. The position of the microtubule pivoting point at time $t(i)$ was measured from the intersection of microtubule traces (reconstructed from the end positions) from two neighboring frames. If the microtubules in the neighboring frames were parallel, the first frame was excluded from further analysis. The length of each end of the microtubule at time $t(i)$ was then calculated as the microtubule end-to-pivot-point lengths $L_1(i)$ and $L_2(i)$. Time courses of L_1 and L_2 were used to calculate microtubule end velocities v_1 and v_2 by linear regression. Translation velocity was taken to be $|(v_1 - v_2)/2|$; the absolute value was computed because the polarity of the microtubules was not independently determined in these experiments. The use of the absolute value in this calculation results in a small positive bias in velocity measurements on nonmoving microtubules (e.g., those in AMP-PNP).
39. We thank E. Young and C. Ding for the initial assay development, A. Hiller for painstaking analysis of microtubule orientation data, and E. Young, L. Hedstrom, C. Miller, M. Welte, and K. Kinosita Jr. for comments on the manuscript. Supported by the National Institute of General Medical Sciences.

4 June 2001; accepted 19 December 2001